Supporting Information for
Uncertainty on Atlantic Niño variability projections

A. Prigent[1], R. A. Imbol Koungue[2], A. S. N. Imbol Nkwinkwa[2], G. Beobide-Arsuaga[3,4], R. Farneti[1]

[1]Earth System Physics Section, The Abdus Salam International Centre for Theoretical Physics (ICTP), Trieste, Italy

[2]GEOMAR Helmholtz Centre for Ocean Research Kiel, Kiel, Germany

[3]International Max Planck Research School on Earth System Modelling, Hamburg, Germany

[4]Institute of Oceanography, Center for Earth System Research and Sustainability (CEN), Universität Hamburg, Hamburg, Germany

Corresponding author: Arthur Prigent (aprigent@ictp.it)

Contents of this file

Text S1. Sources of uncertainties

Adapting from Reintges et al., (2017) and Beobide-Arsuaga et al., (2021), the variable x in (1) represents the Atlantic Niño variability, which depends on the scenario (s), model (m) and time (t):

$$x = x(s, m, t) \quad (1)$$

We consider low-pass filtered values of the Atlantic Niño variability X, i.e. resulting from the 31-year running filter (section 2.3), and decompose it into its long-term trend X_f and internal long-term variability ε:

$$X(s, m, t) = X_f(s, m, t) + \varepsilon(s, m, t) \quad (2)$$

The long-term trend X_f is estimated by a 2nd order polynomial fit calculated over the period 1900-2085. A comparison to higher order polynomial fits is made in Figure S3. The choice of the order of the polynomial fit is important as it represents the response of the Atlantic Niño variability to anthropogenic forcing. While a too high order of the polynomial fit would artificially decrease the internal variability, a too low order would not capture the nonlinear externally forced trend. Under moderate (Figure S3b) and strong (Figure S3c) external forcings (RCP4.5/SSP2-4.5 and RCP8.5/SSP5-8.5, respectively) the different orders yield a similar pattern. Under weak (Figure S3a) external forcing (RCP2.6/SSP1-2.6) only the 2nd order polynomial fit seems to capture the forced trend. Therefore, as in Beobide-Arsuraga et al., (2021), a 2nd order fit has been chosen. The response to the anthropogenic forcing over the period 2005-2085, x_f, is estimated for each model using the corresponding X_{fp} , which is the projected long-term Atlantic Niño variability trend (future projection) over the period 2005-2085 (3). We subtract the historical average i taken over the period 1981-2005 to X_{fp}:

$$x_f(s, m, t) = X_{fp}(s, m, t) - i(s, m) \quad (3)$$

Using the long-term signal anomaly x_f (3), we can define the time-dependent inter-model uncertainty $M(t)$. It corresponds to the spread between the model projections which are then averaged over the three scenarios:

$$M(t) = \frac{1}{N_s} \cdot \sum_s var_m \left(x_f(s,m,t) \right) \quad (4)$$

In our equations, we use a variance operator defined as follows:

$$var_d(p) = \frac{1}{N_d - 1} \cdot \sum_d (p - \frac{1}{N_d} \cdot \sum_d p)^2 \quad (5)$$

Where p is any parameter for which the variance is computed in the dimension d.

The scenario uncertainty is also time-dependent, $S(t)$, and can be defined by averaging x_f over all models for each scenario and by computing the spread among the three of them (6):

$$S(t) = var_s \left(\frac{1}{N_m} \sum_m x_f(s,m,t) \right) \quad (6)$$

Next, the internal variability, I, is estimated by taking the spread of each model's internal variability over the time, and then averaging over all models and scenarios (7):

$$I = \frac{1}{N_s} \cdot \sum_s \frac{1}{N_m} \cdot \sum_m var_t \big(\varepsilon(s,m,t) \big) \quad (7)$$

As the time evolution of the internal variability (Figure S4) shows no relevant differences between different periods, it confirms the choice of a time independent internal variability. It follows that the total uncertainty, T(t), is given by:

$$T(t) = M(t) + S(t) + I \quad (8)$$

Finally, to test whether the global warming signal in Atlantic Niño variability is statistically significant, we use the following signal-to-noise ratio $SNR(t)$ (9) as in Beobide-Arsuaga et al., (2021):

$$SNR(t) = \frac{G(t)}{q_{\frac{c}{2}} \cdot \sqrt{T(t)}} \quad (9)$$

With $G(t)$ being the signal and corresponding to the average of x_f over all models and scenarios (10):

$$G(t) = \frac{1}{N_s} \cdot \sum_s \frac{1}{N_m} \cdot \sum_m x_f(s,m,t) \quad (10)$$

The noise corresponds to the 95th percentile of the standard normal distribution $q_{\frac{c}{2}}$ multiplied by the total uncertainty $T(t)$ (8).

Text S2. Bjerknes feedback

The Bjerknes feedback (Bjerknes, 1969) can be decomposed into three components: the first component (BF1) is the western equatorial Atlantic zonal wind speed anomalies sensitivity to ATL3-averaged SSTA; the second component (BF2) is the eastern equatorial Atlantic thermocline response to ATL4-averaged equatorial Atlantic zonal wind speed anomalies; and the third component (BF3) representing the pointwise SSTA response to thermocline depth variations. Here, SSH anomalies are used as a proxy for thermocline depth variations.

Table S1. List of the CMIP5 models used in this study. 16 grey shaded models have the variables tos, uas and zos available for all scenarios considered. The CO_2 concentration in the year 2100 (Meinhausen et al., 2011) for each RCP is 421 ppm, 538 ppm and 936 ppm, respectively. The CO_2 concentration specified in the abrupt4×CO_2 experiment is four times that in the pre-industrial control runs, which is about 1120 ppm for the CMIP5 models. The standard length of the abrupt4×CO_2 is 150 years.

No.	Models	Historical			RCP2.6			RCP4.5			RCP8.5			Abrupt 4×CO_2		
		tos	uas	zos	tos	uas	zos	tos	uas	zos	tos	uas	zos	tos	uas	zos
1	BCC-CSM1.1	X	X	X	X	X	X	X	X	X	X	X	X	X	X	X
2	CCSM4	X		X	X		X	X		X	X		X	X		X
3	CNRM-CM5	X	X	X	X	X	X	X	X	X	X	X	X	X	X	X
4	CSIRO-Mk3.6.0	X	X	X	X	X	X	X	X	X	X	X	X	X		X
5	CanESM2	X	X	X	X	X	X	X	X	X	X	X	X	X	X	X
6	GFDL-CM3	X	X	X	X	X	X	X	X	X	X	X	X	X	X	X
7	GFDL-ESM2G	X	X	X	X	X	X	X	X	X	X	X	X	X	X	X
8	GFDL-ESM2M	X	X	X	X	X	X	X	X	X	X	X	X	X	X	X
9	GISS-E2-H	X	X		X	X		X	X		X	X		X	X	
10	GISS-E2-R	X	X	X	X	X	X	X	X	X	X	X	X	X	X	X
11	HadGEM2-AO	X	X		X	X		X	X		X	X				
12	HadGEM2-ES	X	X	X	X	X	X	X	X	X	X	X	X	X	X	X
13	IPSL-CM5A-LR	X	X	X	X	X	X	X	X	X	X	X	X	X	X	X
14	IPSL-CM5A-MR	X	X	X	X	X	X	X	X	X	X	X	X	X	X	X

15	MIROC-ESM	X	X	X	X	X	X	X	X	X	X	X	X	X	X	X
16	MIROC-ESM-CHEM	X	X	X	X	X	X	X	X	X	X	X	X			
17	MIROC5	X	X	X	X	X	X	X	X	X	X	X	X	X	X	X
18	MPI-ESM-LR	X	X	X	X	X	X	X	X	X	X	X	X	X	X	X
19	MPI-ESM-MR	X	X	X	X	X	X	X	X	X	X	X	X	X	X	X
20	MRI-CGCM3	X	X	X	X	X	X	X	X	X	X	X	X	X	X	X
21	NorESM1-M	X	X	X	X	X	X	X	X	X	X	X	X	X	X	X
22	NorESM1-ME	X	X	X	X		X	X	X	X	X		X	X		X

Table S2. List of the CMIP6 models used in this study. 18 grey shaded models have the variables tos, uas and zos available for all scenarios considered. The CO_2 concentration in the year 2100 (Meinhausen et al., 2020) for each SSP is 445.6 ppm, 602.8 ppm and 1135.2 ppm, respectively. The CO_2 concentration specified in the abrupt4×CO_2 experiment is four times that

in the pre-industrial control runs, which is about 1136 ppm for the CMIP6 models. The standard length of the abrupt4×CO_2 is 150 years.

No.	Models	Historical			SSP1-2.6			SSP2-4.5			SSP5-8.5			Abrupt 4×CO_2		
		tos	uas	zos	tos	uas	zos	tos	uas	zos	tos	uas	zos	tos	uas	zos
1	ACCESS-CM2	X	X	X	X	X	X	X	X	X	X	X	X	X	X	X
2	ACCESS-ESM1-5	X	X	X	X	X	X	X	X	X	X	X	X	X	X	X
3	BCC-CSM2-MR	X	X	X	X	X	X	X	X	X	X	X	X	X	X	X
4	CAMS-CSM1-0	X	X	X	X	X	X	X	X	X	X	X	X	X	X	X
5	CAS-ESM2-0	X	X	X	X	X	X	X	X	X	X	X	X	X	X	X
6	CMCC-CM2-SR5	X	X	X	X	X	X	X	X	X	X	X	X	X	X	X
7	CMCC-ESM2	X	X	X	X	X	X	X	X	X	X	X	X	X	X	X
8	CanESM5	X	X	X	X	X	X	X	X	X	X	X	X	X	X	X
9	EC-Earth3	X	X	X	X	X	X	X	X	X	X	X	X			
10	EC-Earth3-Veg	X	X	X	X	X	X	X	X	X	X	X	X	X	X	X
11	EC-Earth3-Veg-LR	X	X	X	X	X	X	X	X	X	X	X	X	X	X	X
12	FGOALS-f3-L	X	X	X	X	X		X	X		X	X		X	X	X
13	FGOALS-g3	X		X	X		X	X		X	X		X			X
14	FIO-ESM-2-0	X		X	X		X	X		X	X		X	X		X
15	GFDL-ESM4	X	X	X	X	X	X	X	X	X	X	X	X	X		X
16	INM-CM4-8	X	X	X	X	X	X	X	X	X	X	X	X	X	X	X
17	INM-CM5-0	X	X	X	X	X	X	X	X	X	X	X	X	X	X	X
18	IPSL-CM6A-LR	X	X	X	X	X	X	X	X	X	X	X	X	X	X	X
19	KIOST-ESM	X	X	X	X	X	X	X	X	X	X	X	X	X	X	X
20	MIROC6	X	X	X	X	X	X	X	X	X	X	X	X	X	X	X
21	MPI-ESM1-2-HR	X	X	X	X	X	X	X	X	X	X	X	X	X	X	X
22	MPI-ESM1-2-LR	X	X	X	X	X	X	X	X	X	X	X	X	X	X	X
23	MRI-ESM2-0	X	X	X	X	X	X	X	X	X	X	X	X	X	X	X
24	NESM3	X	X	X	X	X	X	X	X	X	X	X	X	X		X
25	NorESM2-LM	X		X	X		X	X		X	X		X	X		X
26	NorESM2-MM	X		X	X		X	X		X	X		X	X		X
27	TaiESM1	X		X	X		X	X		X	X		X			X

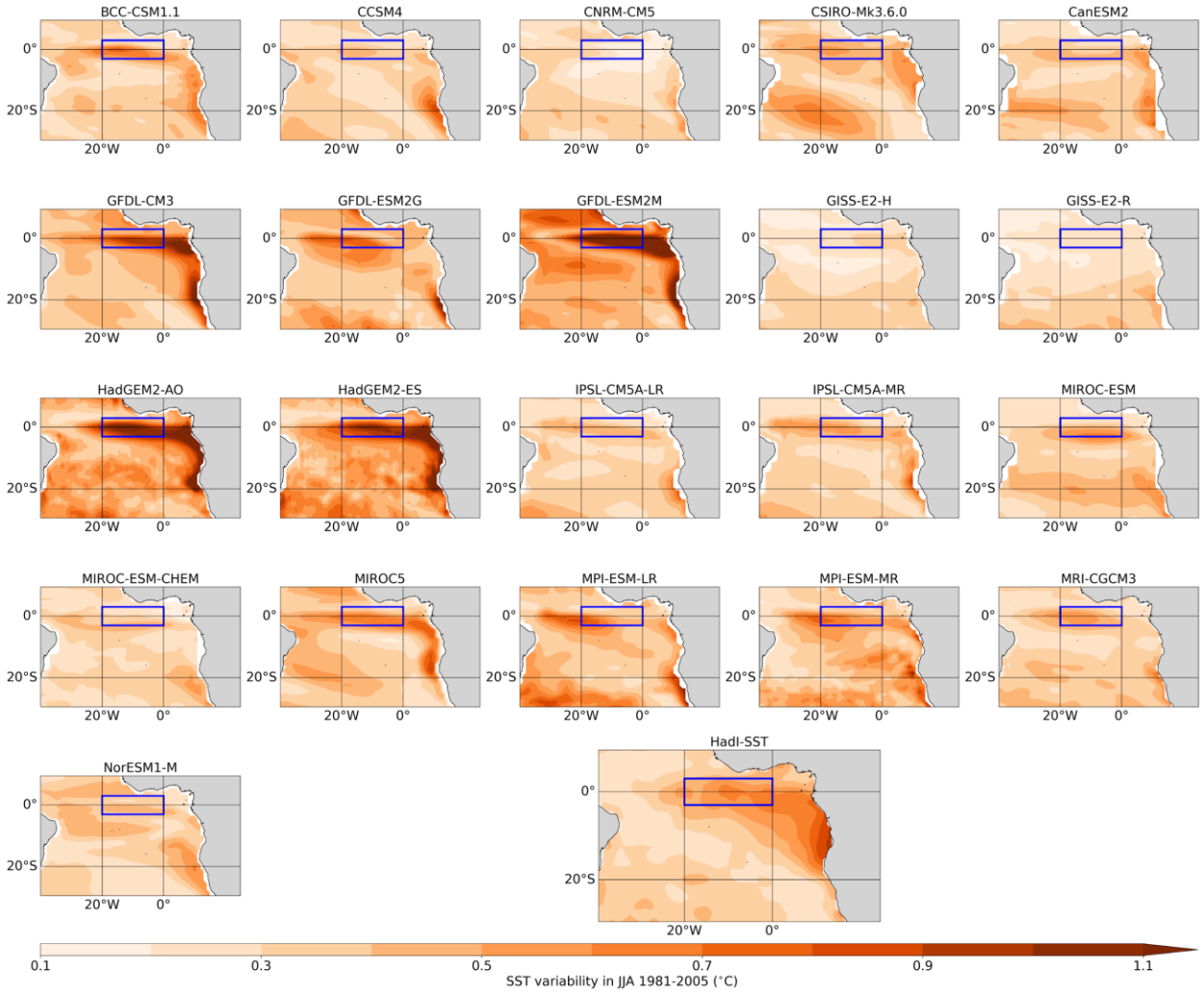

Figure S1. Standard deviation of the JJA-averaged SST anomalies over the period 1981-2005 for each CMIP5 model used in this study and for HadI-SST.

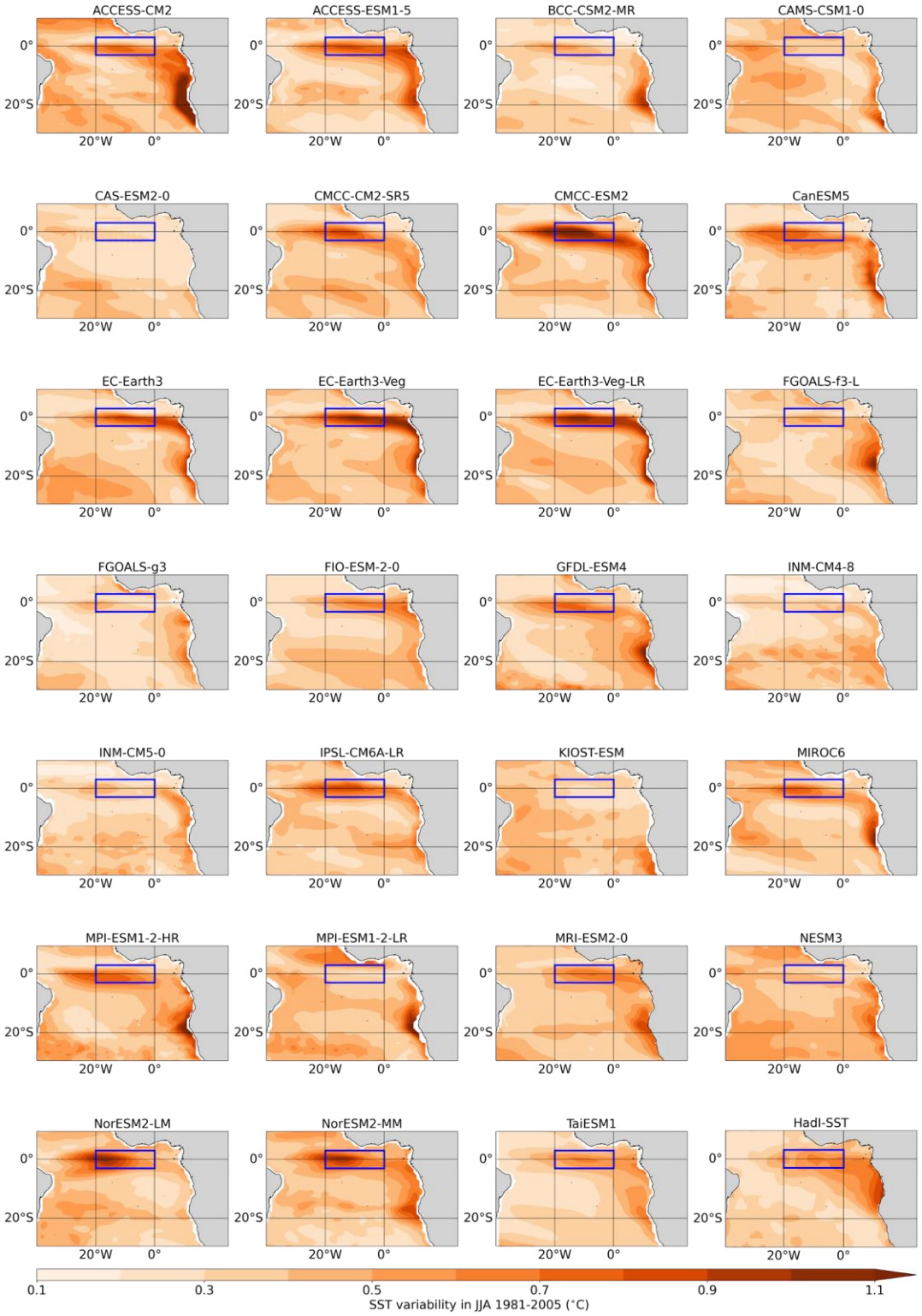

Figure S2. Standard deviation of the JJA-averaged SST anomalies over the period 1981-2005 for each CMIP6 model used in this study and for HadI-SST.

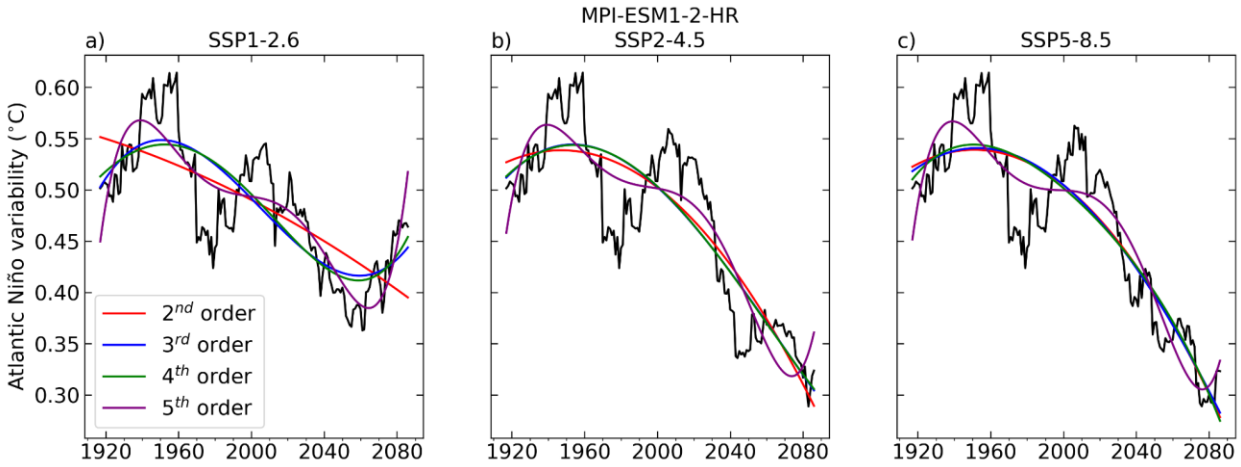

Figure S3. Historical and projected Atlantic Niño variability for the MPI-ESM1-2-HR model (black) with the 2nd (red), 3rd (blue), 4th (green) and 5th (purple) order polynomial fits: in (a, b, c) for the SSP1-2.6, SSP2-4.5, SSP5-8.5 scenarios, respectively.

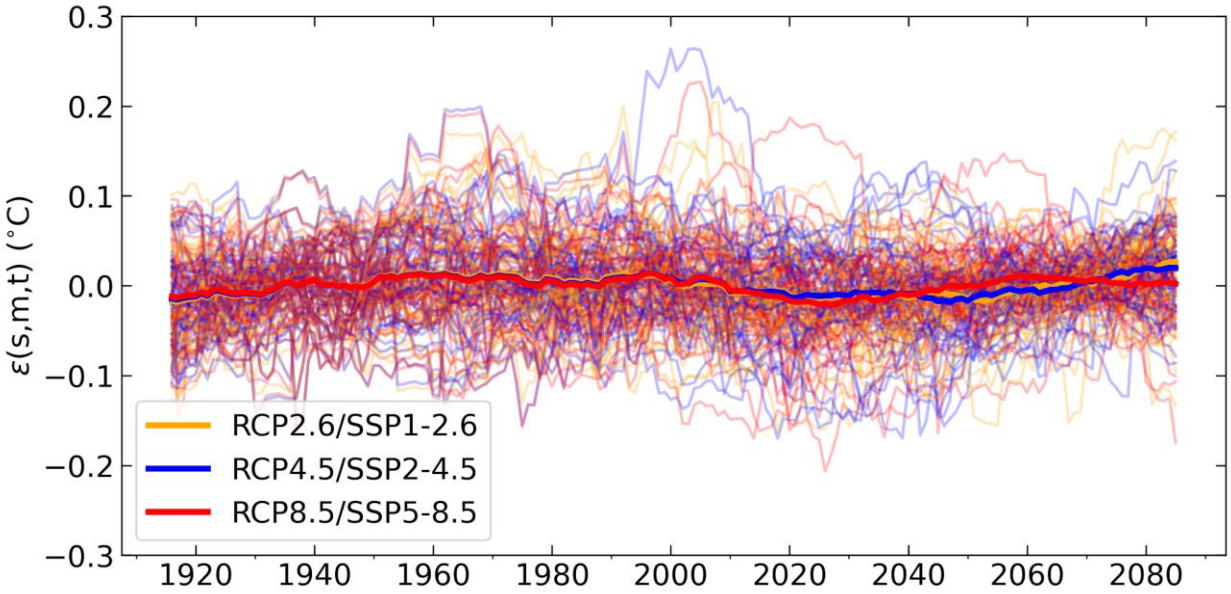

Figure S4. Internal long-term Atlantic Niño variability for each model and scenario $\varepsilon(s,m,t)$ (2), defined as the difference between the Atlantic Niño variability, $X(s,m,t)$, and the 2nd order polynomial fit $Xf(s,m,t)$. Orange, blue and red lines represent the RCP2.6/SSP1-2.6, RCP4.5/SSP2-4.5 and RCP8.5/SSP5-8.5 scenarios, respectively. Thick solid lines are the scenario means.

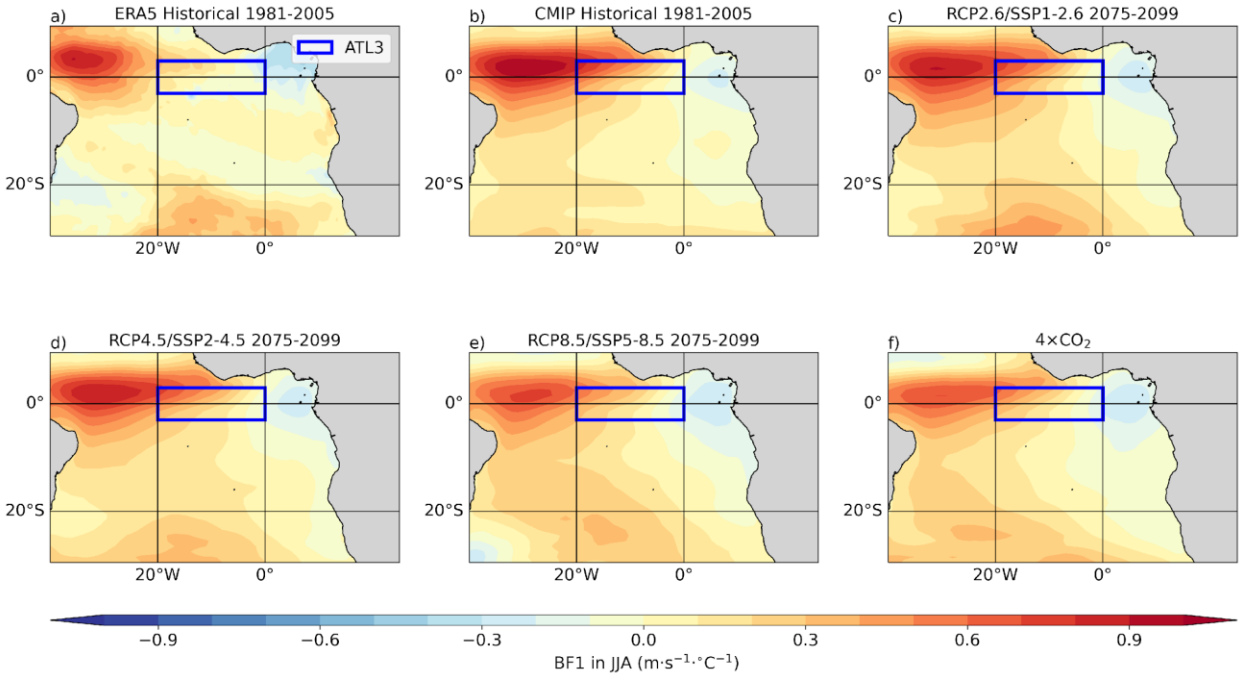

Figure S5. First component of the Bjerknes feedback (BF1) in JJA, zonal wind anomalies sensitivity to SST anomalies in the ATL3 region. (a) BF1 estimated using ERA5 over the period 1981-2005. (b) BF1 estimated using the CMIP5 and CMIP6 ensemble mean over the period 1981-2005. (c) Same as (b) but for the scenario RCP2.6/SSP1-2.6 over the period 2075-2099. (d) Same as (b) but for the scenario RCP4.5/SSP2-4.5. (e) Same as (b) but for the scenario RCP8.5/SSP5-8.5. (f) Same as (b) but for the abrupt4×CO_2 scenario. Ensemble means are composed of 34 models, 16 CMIP5 and 18 CMIP6 models (Tables S1 and S2), for which the variables tos, uas, and zos are available for each scenario: historical, RCP2.6, RCP4.5, RCP8.5, SSP1-2.6, SSP2-4.5, SSP5-8.5 and abrupt4×CO_2.

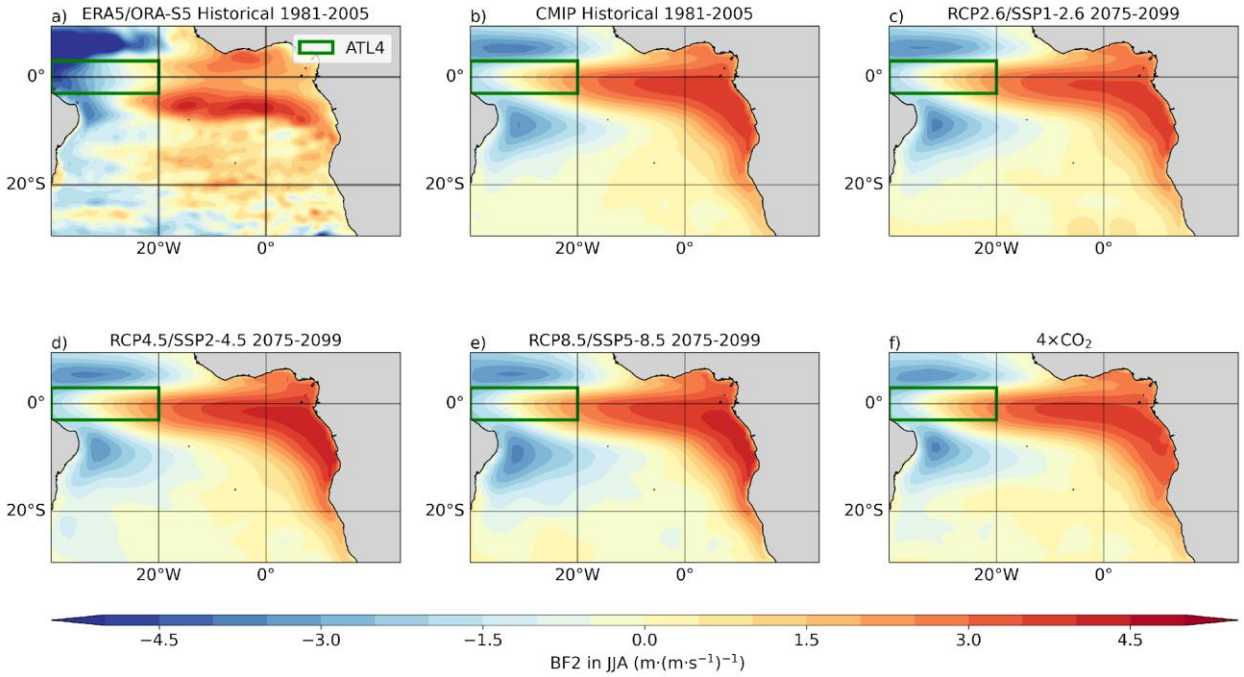

Figure S6. Second component of the Bjerknes feedback (BF2) in JJA, sea surface height (SSH) anomalies sensitivity to zonal wind anomalies in the ATL4 region. (a) BF2 estimated using ERA5 zonal winds and ORA-S5 SSH over the period 1981-2005. (b) BF2 estimated using the CMIP5 and CMIP6 ensemble mean over the period 1981-2005. (c) Same as (b) but for the scenario RCP2.6/SSP1-2.6 over the period 2075-2099. (d) Same as (b) but for the scenario RCP4.5/SSP2-4.5. (e) Same as (b) but for the scenario RCP8.5/SSP5-8.5. (f) Same as (b) but for the abrupt4×CO_2 scenario. Ensemble means are composed of 34 models, 16 CMIP5 and 18 CMIP6 models (Tables S1 and S2), for which the variables tos, uas, and zos are available for each scenario: historical, RCP2.6, RCP4.5, RCP8.5, SSP1-2.6, SSP2-4.5, SSP5-8.5 and abrupt4×CO_2.

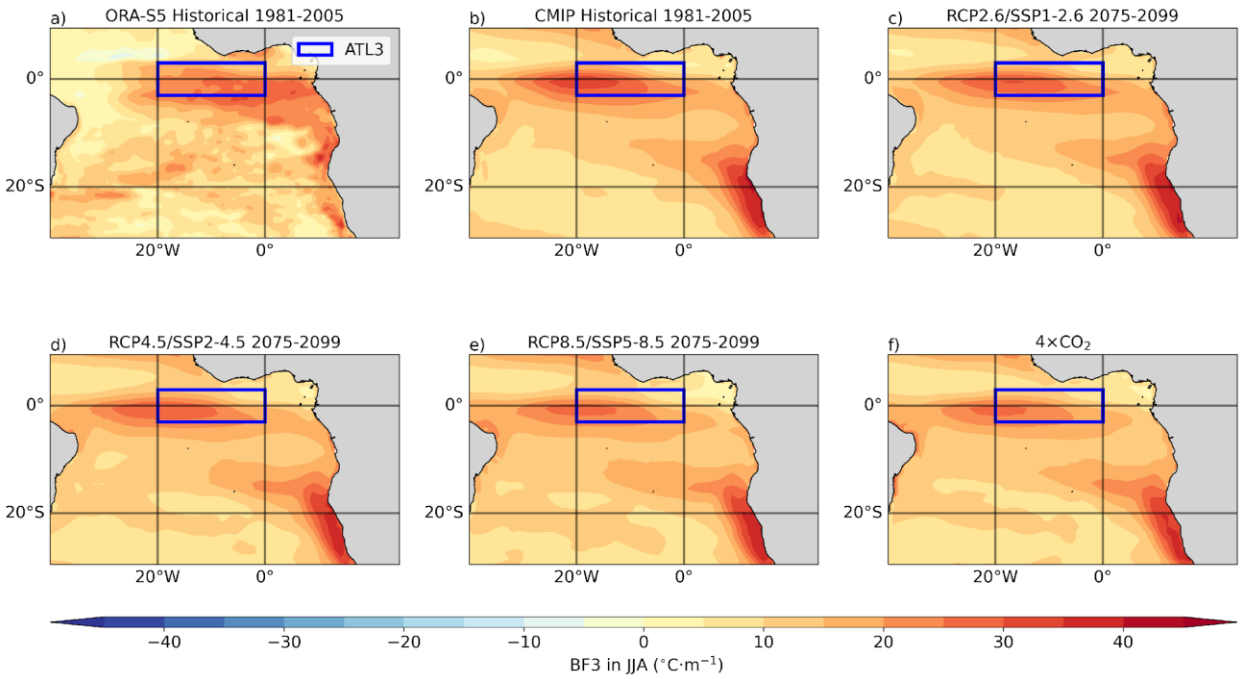

Figure S7. Third component of the Bjerknes feedback (BF3) in JJA, sea surface temperature (SST) anomalies sensitivity to SSH anomalies pointwise. (a) BF3 estimated using ORA-S5 SST and ORA-S5 SSH over the period 1981-2005. (b) BF3 estimated using the CMIP5 and CMIP6 ensemble mean over the period 1981-2005. (c) Same as (b) but for the scenario RCP2.6/SSP1-2.6 over the period 2075-2099. (d) Same as (b) but for the scenario RCP4.5/SSP2-4.5. (e) Same as (b) but for the scenario RCP8.5/SSP5-8.5. (f) Same as (b) but for the abrupt4×CO_2 scenario. Ensemble means are composed of 34 models, 16 CMIP5 and 18 CMIP6 models (Tables S1 and S2), for which the variables tos, uas, and zos are available for each scenario: historical, RCP2.6, RCP4.5, RCP8.5, SSP1-2.6, SSP2-4.5, SSP5-8.5 and abrupt4×CO_2.

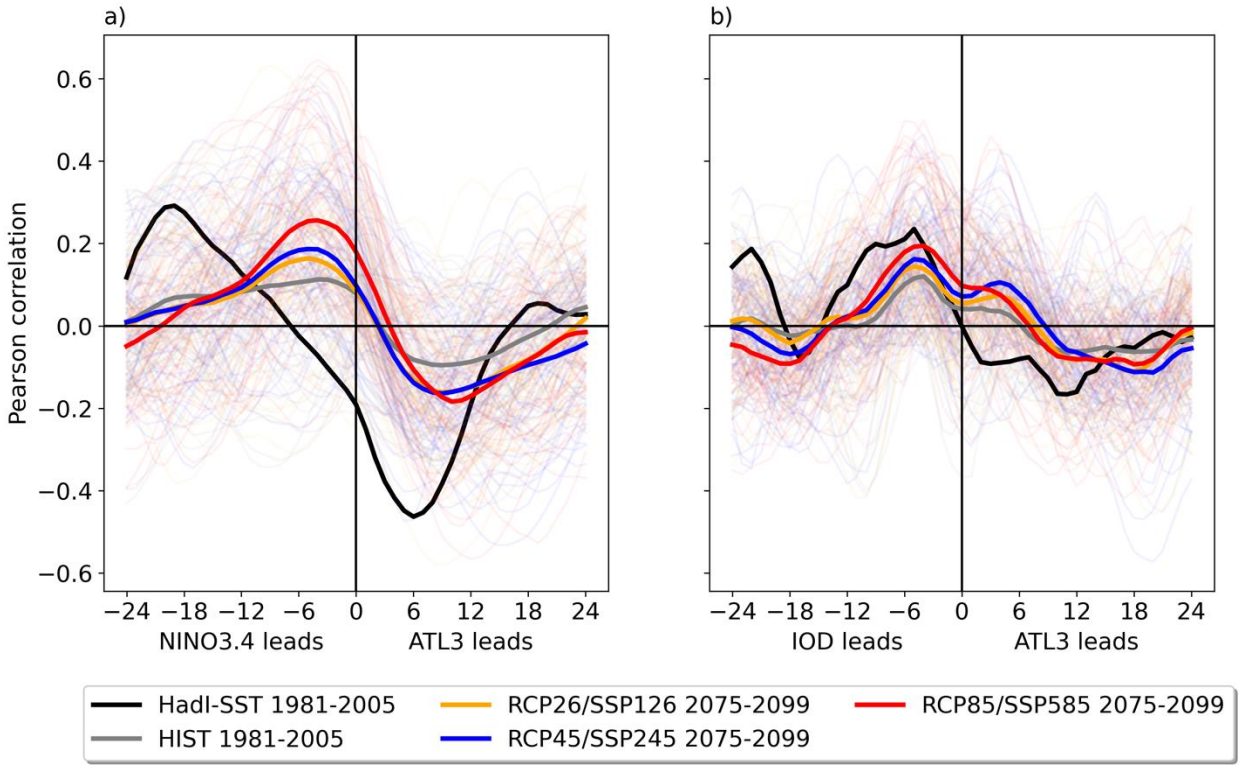

Figure S8. Cross-correlations between: (a) ATL3-averaged SSTA and NINO3.4-averaged SSTA and (b) ATL3-averaged SSTA and IOD index. The thick black lines represent the cross-correlations computed with HadI-SST over the period 1981-2005. The thick grey lines are the ensemble mean cross-correlations when considering all CMIP5 and CMIP6 models over the period 1981-2005. The thin grey lines are the cross-correlations for each model over the period 1981-2005. The thick orange, blue and red lines are the ensemble mean cross-correlations when considering all CMIP5 and CMIP6 models over the period 2075-2099 for the scenarios RCP2.6/SSP1-2.6, RCP4.5/SSP2-4.5 and RCP8.5/SSP5-8.5, respectively. The corresponding thin orange, blue and red lines are the cross-correlations for each model over the period 2075-2099. The NINO3.4 box is defined from 170˚W to 120˚W and from 5˚S to 5˚N. The IOD index is represented by the anomalous SST gradient between the western equatorial Indian Ocean (50˚E-70˚E; 10˚S-10˚N) and the south eastern equatorial Indian Ocean (90˚E-110˚E; 10˚S-0˚N).

References

Beobide-Arsuaga, G., Bayr, T., Reintges, A. *et al.* Uncertainty of ENSO-amplitude projections in CMIP5 and CMIP6 models. *Clim Dyn* **56,** 3875–3888 (2021). https://doi.org/10.1007/s00382-021-05673-4

Bjerknes, J. (1969). Atmospheric teleconnections from the equatorial Pacific, *Monthly Weather Review*, *97*(3), 163-172. doi: https://doi.org/10.1175/1520-0493(1969)097<0163:ATFTEP>2.3.CO;2

Meinshausen, M., Smith, S.J., Calvin, K. *et al.* The RCP greenhouse gas concentrations and their extensions from 1765 to 2300. *Climatic Change* **109**, 213 (2011). https://doi.org/10.1007/s10584-011-0156-z

Meinshausen, M., Nicholls, Z. R. J., Lewis, J., Gidden, M. J., Vogel, E., Freund, M., Beyerle, U., Gessner, C., Nauels, A., Bauer, N., Canadell, J. G., Daniel, J. S., John, A., Krummel, P. B., Luderer, G., Meinshausen, N., Montzka, S. A., Rayner, P. J., Reimann, S., Smith, S. J., van den Berg, M., Velders, G. J. M., Vollmer, M. K., and Wang, R. H. J.: The shared socio-economic pathway (SSP) greenhouse gas concentrations and their extensions to 2500, Geosci. Model Dev., 13, 3571–3605, https://doi.org/10.5194/gmd-13-3571-2020, 2020.

Reintges A, Martin T, Latif M, Keenlyside NS (2017) Uncertainty in twenty-first century projections of the Atlantic Meridional Overturning Circulation in CMIP3 and CMIP5 models. Clim Dyn 49:1495–1511. https://doi.org/10.1007/s00382-016-3180-x